# A Stable Hybrid Potential–SPH Technique to Enforce the Fluid Incompressibility

JUAN J. PEREA
University of Seville
School of Computer Engineering
Avda. Reina Mercedes, s/n, 41012 Sevilla
SPAIN
jperea@us.es

JUAN M. CORDERO
University of Seville
School of Computer Engineering
Avda. Reina Mercedes, s/n, 41012 Sevilla
SPAIN
jmcordero@us.es

*Abstract:* The SPH method has extensively used in fluid flow simulation. Through SPH the fluid is modelled by a particles system whose mutual interaction is weighed by a function, named kernel function, whose limits define the neighbouring of each particle. In spite of the high capabilities of SPH for simulate complex environments, it shows shortcomings specially if the fluid is subject to high changes in the pressure, the velocity and the density as occur in phenomena such as shock–tube, blast–wave or in the boundary and discontinuities where the number of neighbour particles is relatively low. In this case, the pressure gradient is inaccurate. As consequence, the simulation is instable with an erratic behaviour of particles. To avoid this problem, we propose a hybrid technique. This one consists in formulating the pressure gradient from a potential defined on each particles pair. Thus, the pressure gradient is immune to the low number of neighbour particles. Also, our proposal allows enforcing the fluid incompressibility. To show the improvements obtained we will carry out a set of simulations.

*Key–Words:* fluid simulation, SPH, stability, accuracy, potential–based.

## 1 Introduction

The fluid flow simulation plays an essential role in several disciplines both the scientific and technical. From an analytic point of view, it is formulated by Fluid Mechanics that set the partial differential equations describing the fluid flow. However, its complexity only allows obtaining analytic results for a restricted set of cases with high spatial symmetry. In most cases, the numerical methods must be used. These ones are studied by Computational Fluid Dynamic (CFD). Through CFD, the partial differential equations, are transformed into a set of algebraic equations, whose solution allow simulating the fluid flow. One of these methods is *Smoothed Particle Hydrodynamics* (SPH) which is widely used for its adaptability and versatility [21, 32].

SPH operates on fluid discretization through particles that interact among themselves. Thus, it is based on the Lagrangian formulation. Descriptively, each particle depicts a discrete portion of the continuum fluid and moves with the flow. In this methodology, the dynamic quantities are fit on each particle and its mutual interaction is weighed by a scalar function dependent on distance. This function, known as *kernel function*, must satisfy a set of analytical properties such as it must be monotonically decreasing, it must be normalized and its domain, named *supported domain*, should be limited. Each particle has got an associated kernel function, whose supported domain limits the number of neighbour particles.

The SPH method has highlight features such as the conservation of mass [13, 19, 21], its adaptability and versatility to simulate complex environments [19] and the simplification of the formulation to solve the fluid dynamic equations [9, 13]. Nevertheless, despite these advantages, the simulation by SPH can show stability problems that affect the realism of simulation [3, 6, 28]. There are several instabilities types: the local mixing instability (LMI) [25], the heating instability [25], but the most remarkable is related to pressure gradient [20, 24, 25]. The inaccuracy of pressure gradient induces a tensile instability [14, 18, 21] or pairing of particles [2, 3, 24].

There is a consensus that relates the instability of pressure gradient and the number of neighbouring particles, specially when this number is relatively low or the particles distribution is not smooth [3, 10, 21, 24, 28]. According the number of neighbouring particles decreases, the inaccuracy of pressure force is increased. Consequently, the particles are scattered and show erratic behaviour. Usually, it has been regarded that increasing the radius of the supported domain the inaccuracy is reduced. Nevertheless, the increase in the supported domain re-

duces the resolution and, as consequence, the accuracy [3, 21, 32]. Furthermore, there are regions, such as the boundaries of fluid or its discontinuities, where the number of neighbour particles cannot be increased [28]. Other methodologies have been developed to avoid the problems associated to the low number of neighbouring. These techniques either reformulate the dynamic equations modelled by SPH [21, 25] or positioning control points to reduce the effects of the external loads on the pressure gradient [4, 33]. Nevertheless, these proposals show shortcomings since can violate the conservation of momentum [3, 16], particularly in boundaries and discontinuity regions. Also, they are only effective under specific conditions, if these conditions are not satisfied, an erroneous overdamping is induced [3].

To avoid these shortcomings related to the pressure force and the incompressibility enforcement, we propose a hybrid technique potential–SPH. Succinctly, our proposal is based on a formulation of a conservative potential that allow us to derive the pressure force. The constraints to obtain this force has the aim the improving the stability and accuracy specially in the discontinuities and boundary regions. On the other hand, the formulated pressure force allow us to enforce incompressibility without the need to use a predictor–corrector process what improves the efficiency. To show the improvements that our proposal allows obtaining, we will carry out a set of test usually used to quantify the stability and accuracy.

## 2 SPH Method

The SPH method, initially developed by Gingold and Monaghan [5] and Lucy [11], was formulated from the integral formulation of the delta Dirac function [13].

$$f(r) = \int f(r')\delta(r - r')dr', \tag{1}$$

where $f$ depicts any scalar function and $\delta$ is the delta Dirac function.

According to the interpolation theory, the function $\delta$ can be replaced by a function with spatial extension. Thus, the integral expression (1) can be reformulated by the below equation.

$$f(r) = \int_\Omega f(r')W(r - r', h)dr' + \mathcal{O}(h^2), \tag{2}$$

where $W$ is named the kernel function, $\Omega$ refers to the volume of the definition domain of $W$ and $h$ is the radius of the supported domain.

Regarding the kernel function, this one must satisfy, at least, the following constraints:

1. It must be normalized and tend to $\delta$ when $h$ tends to zero, i.e:

$$\lim_{h\to 0} W(r - r', h) = \delta(r - r'); \int_V W dV' = 1. \tag{3}$$

2. It must be positive and decrease continuously with $(r - r')$.

3. It must be symmetric with respect to $(r - r')$.

Quantitatively, the modelling of a continuous medium using a particles system entails transforming the integral, equation (2), by a sum where the mass of each particle depicts a volume element whose mass is $\rho dV$, i.e:

$$\begin{aligned}\langle f(r)\rangle &= \int_\Omega \frac{f(r')}{\rho(r')} W(r - r', h)\rho(r')dr' \\ &\approx \sum_{j\in\mathcal{N}(i)} m_j \frac{f_j}{\rho_j} W(r_j - r_i, h),\end{aligned} \tag{4}$$

where $\langle\rangle$ refers to the approximated value of function $f$ since the second order term has not been considered, $\mathcal{N}(i)$ depicts the neighbour particles $j$ of each particle $i$ and $\rho_j$ is the mass density allocated to the particle $j$.

From the symmetry property (item 3), the gradient of any scalar magnitude $f(r)$ can be simplified as:

$$\begin{aligned}\langle \nabla f(r)\rangle &= \frac{\partial}{\partial r} \int \frac{f(r')}{\rho(r')} W(r - r', h)\rho(r')dr' \\ &\approx \sum_{j\in\mathcal{N}(i)} m_j \frac{f_j}{\rho_j} \nabla W(r_j - r_i, h).\end{aligned} \tag{5}$$

Generalizing the equation (5), it is possible to formulate a valid equation for any differential order. This generalized equation is:

$$\langle \nabla^l f(r_i)\rangle = \sum_{j\in\mathcal{N}(i)} m_j \frac{f_j}{\rho_j} \nabla^l W(r_j - r_i, h), \tag{6}$$

where $l$ refers to the differential order equation.

It is noted that the equation (6) does not regard the second order term [21]. Also, it violates the conservation of angular momentum [13]. As consequence, although the equation (6) satisfies the SPH premises, the accuracy of the obtained results can be compromised. To prevent this issue, this equation must be modified to be applied to fluid flow simulation, according is described by [13]. Nevertheless, this symmetrical formulation can increase the instability [2, 7, 21].

# 3 Dynamic Equations

The dynamic of an incompressible and inviscid fluid, whose flow evolves adiabatically with high Reynolds number is described by the below PDEs system:

$$\nabla \cdot v = 0, \tag{7}$$

$$\frac{Dv}{Dt} = -\frac{1}{\rho}(\nabla p) + F, \tag{8}$$

where $D/Dt = \partial/\partial t + v \cdot \nabla$ refers to the convective derivative, $\rho$ is the mass density, $v$ is the velocity, $p$ is the pressure and $F$ depicts the body force vector per unit volume.

To close this system of equations, it is necessary to regard a relationship between the pressure and the mass density. This relationship is set by the equation of state (EOS). Although there are several formulations of the EOS, in SPH is usually used Tait's equation expressed as:

$$p = (\gamma - 1)\rho, \tag{9}$$

where $\gamma$ is the adiabatic index.

The modelling of the equations (7) and (8) by SPH shows problems of stability and accuracy. To solve these problems, several proposals have been developed [15, 21, 23, 30]. The most outstanding are the research developed by Price [21], appointed as MPM, and the technique described by Inutsuka [7] known as GPSH.

Regarding the variational approach, Price [21] models the equation (8) as:

$$\frac{dv_i}{dt} = -\sum_{j\in\mathcal{N}(i)} m_j \left(\chi_i \nabla W_{ij}(h_i) + \chi_j \nabla W_{ij}(h_j)\right) + \sum_{j\in\mathcal{N}(i)} \alpha \frac{m_i}{\rho_{ij}} v_s \, v_{ij} \cdot \hat{R}_{ij} \nabla \tilde{W}_{ij} + F \tag{10}$$

where the subscript $i$ and $j$ refers to particle $i$ and $j$ respectively, $\chi = (\Omega^{-1} p/\rho^2)$, $\Omega$ is a correction term related to the smoothing length, $\hat{R}_{ij}$ is the unit vector defined by the line joining the particles $i$ and $j$, $\tilde{W}_{ij}$ is the averaged kernel and $v_s = c_i + c_j - v_{ij} \cdot \hat{R}_{ij}$. In Price [21] is shown a detailed explanation of the derivation of this equation.

On the other hand, the technique GSPH is seeking to restore consistency for the discrete density estimate by the kernel function convolutions using a Riemann solver. According to the GSPH technique, the equation (8) is formulated as:

$$\frac{dv_i}{dt} = -\sum_{j\in\mathcal{N}(i)} m_j p^*_{ij} \left[V^2_{ij}(h_i)\nabla W_{ij}(h_i\sqrt{2}) + V^2_{ij}(h_j)\nabla W_{ij}(h_j\sqrt{2})\right] \approx -\sum_{j\in\mathcal{N}(i)} m_j p^*_{ij} \left(\frac{1}{\rho_i^2}\nabla \tilde{W}_{ij} \frac{1}{\rho_j^2}\nabla \tilde{W}_{ij}\right) + F \tag{11}$$

where $p^*$ is the intermediate pressure arising from the solution of a Riemman solver particularized to the particles pair $i, j$ and $V_{ij}$ are the intermediate velocities related to the solution of Riemann solver particularized to two particles [24]. The papers [7, 8] show a detailed explanation of the derivation of the equation (11).

# 4 Proposed Model

In this section, it will be described the features of our proposal to improve the stability and accuracy of SPH simulations. Firstly, the fundamental hypothesis of the model will be set. From this hypothesis will be formulated our proposal to obtain the pressure force. Next, it will be described the analytic features that should be satisfied by the pressure force to guarantee stability. These features are set from the most outstanding studies in stable simulations scope by SPH. From these constraints and the fundamental hypothesis, it will be formulated the pressure force. Its formulation will allow enforcing the incompressibility. Once the incompressibility is enforced, it will be explained the process to calculate the density using both the SPH formulation and the pressure force. This joined formulation allows fulfilling the incompressibility constraint.

Analytically, when external forces acting on a fluid, the distances between adjacent regions change. Then, into the fluid appears a force that tends to restore the balance conditions [34]. This internal force is quantified by the pressure gradient. Extrapolating this criterion to the modelled fluid by a particle system, we can formulate our fundamental hypothesis, namely: *the pressure force is due to change of the distance between particles.*

Taking into account this premise, we avoid the problems of stability related to modelling of the pressure gradient by SPH, especially when the number of neighboring particles is low [3, 22]. Furthermore, we can enforce the incompressibility constraint on the pressure force and the density. On the other hand, as the force only depends on distance, we can formulate it from a conservative potential [34]. Nevertheless,

any conservative potential is not valid to obtain stable fluid simulations. To set a suitable formulation must be taking into account the constraints that guarantee the stability. These constraints it will be described below.

### 4.1 Pressure Force

Several research have been carried out to set the relationship between stability–accuracy and the pressure gradient. The most highlighting studies assert that the pressure force:

1. It should ensure stability for a wide range of the number of neighbour particles. This feature can be deduced from the studies developed by [3, 12, 21, 28]. These research assert that if the number of particles is too low, the simulations show an erratic scattering of particles, mainly in the boundary of fluid. On the other hand, if the number of particles is high, a clustering of particles can appear.

2. It should be concave in respect of the abscissa axis. This constraint is deduced from the research developed by [1, 3, 24], where is described that a kernel function whose gradient, that appear in pressure force, shows an inflection point and concavity, improve the stability.

3. It should show an asymmetric profile with regard to the minimum value of the force. Thus, two requirements are satisfied: firstly, the repulsive force is increased when the distance is decreased, as it can be deduced from [9] and lastly, the interaction can be weighed by the distance, as is suggested by [3, 21]. A harmonic force can only satisfy the first condition but it would not ensure the last one [21].

4. It should allow us to enforce the incompressibility [12, 28], namely, its formulation should limit the minimum distance among particles. Thus, the formulated force should show an asymptotic behavior with distance. Its aim would be to avoid that the distance between particles will be incompatible with incompressibility constraint.

From these features, we formulate the conservative potential, from which, we will obtain the pressure force. The proposed potential is:

$$V_i(r_i) = \frac{21}{24\pi h_i} \sum_{j \in \mathcal{N}(i)} \left( \frac{2}{\left(R_{ij} - 0.9\varepsilon\right)^2} - \frac{7\pi^2}{2\zeta\left(R_{ij} - (0.85\varepsilon)\right)} + (3\pi^2\sigma) \right), \tag{12}$$

where $R_{ij} = r_j - r_i$, $\varepsilon$ is named as *asymptotic factor*, that allows us to control the incompressibility rate, $\zeta$ is appointed as *depth factor*, by this magnitude, we can avoid the particles clustering and $\sigma$ is named as *tail coefficient*, by means of this coefficient, it is possible to control the potential at the boundary of the supported domain. Empirically, we have evaluated the value range, of these parameters, that offer the best results, these values are: $0.3h \leq \varepsilon \leq h$, $0.5 \leq \zeta \leq 2.0$ and $0.8 \leq \sigma \leq 2.25$. The Figure 1 shows the profile of the formulated potential.

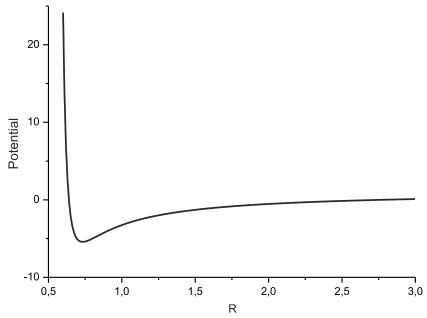


Figure 1: Graph of the proposed potential. The parameter values are $h = 3$, $\varepsilon = 0.6$, $\zeta = 1.25$ and $\sigma = 1.0$.

Analytically the potential, equation (12), only depends on position. As consequence, the force that is derived can be written as $\vec{F}_{p_i} = -\nabla V(r_i)$, i.e:

$$\vec{F}_{p_i} = -\frac{5.25}{6\pi h_i} \sum_{j \in \mathcal{N}(i)} \left( \frac{3.5\pi^2}{\zeta\left(R_{ij} - (0.85\varepsilon)\right)^2} - \frac{4}{\left(R_{ij} - 0.9\varepsilon\right)^3} \right) (h - R_{ij}) \frac{\vec{R}_{ij}}{R_{ij}}, \tag{13}$$

From the Figure 1, we can describe the features of our proposed potential. Firstly, it shows a concavity in respect of the abscissa, as it was established in item 2. Secondly, it shows an asymmetric profile with respect to minimum of force, according to the item 3. Lastly, as a consequence of asymptotic limit, for low values of $r$, we can control the incompressibility, as it was required in item 4. It is noted, as consequence of the pressure force is derived from this potential, this features will be inherited. On the other hand, analyzing the equation (13) we can say that the force is saturated with the distance [34]. Furthermore, this saturation is weighed by the distance. Thus, the pressure force satisfies the constraint suggested by [3, 13, 17, 32]. Also,

the force formulated in equation (13) satisfies the conservation of momentum.

Then, once the pressure force has been obtained, we are going to describe our proposal to control the incompressibility, taking advantage of the asymptotic limit shown by the formulated pressure force.

Due to the fact that the pressure force is obtained from a potential, our technique will hereinafter be referred to as *P–SPH*.

### 4.2 The Enforcement of the Incompressibility

Qualitatively, the incompressibility is related to the maximum force that can be borne by the fluid, without changing its local volume [34]. According to this fact, the incompressibility in a fluid modelled by a particle system can be explained as the minimum distance that the particles can approach. In this context, the force calculated by the equation (13), allows us to model the incompressibility by the asymptotic value when $R$ is low. Nevertheless, if the incompressibility coefficient is lower than $2\%$, we must introduce a control process to reduce the numerical errors accumulated in each time step.

Our proposal to control the incompressibility when its coefficient lower than $2\%$ can be divided into two stages. In the first stage, the pressure force is calculated by the equation (13). In the last stage, we check the particles whose pressure force violates the incompressibility constraint. If the pressure force of any particle violates the incompressibility constraint, then the force excess is quantified and both the dynamic and the position of these particles are modified to satisfy the incompressibility constraint.

To implement this process, firstly we calculate the maximum compression force, namely, the value from which the incompressibility constraint is violated. To this end, we particularize the equation (13) with a distance, whose value is in line with the rest density fluid. According to this description, the obtained equation is:

$$\vec{F}^C_{j|i} = -\frac{5.25}{6\pi h}\left(\frac{3.5\pi^2}{\zeta\left(\xi-(0.85\varepsilon)\right)^2}-\frac{4}{\left(\xi-0.9\varepsilon\right)^3}\right)\frac{\vec{R}}{R}, \tag{14}$$

where $\vec{F}^C_{j|i}$ is the maximum of compression force that the particle $j$ can acquire in respect to particle $i$ and $\xi$ is the minimum distance that the particle $j$ can approximate of particle $i$ without violates the incompressibility. The equation that satisfies this criteria is:

$$\xi = \sqrt[3]{\frac{3m}{4\pi(1-\eta)\rho_0}}, \tag{15}$$

where $\eta$ is the compressibility coefficient and $\rho_0$ is the rest density.

If $|\vec{F}^C_{j|i}| > |\vec{F}_{p_{j|i}}|$, then, we have to control the incompressibility. Thus, we change the force of the particle $j$ and its position, to the maximum tolerated values, i.e.:

$$\vec{F}_{p_{j|i}} = \vec{F}^C_{p_{j|i}} \;\; y \;\; \vec{r}'_j = \xi\frac{\vec{R}}{R}, \tag{16}$$

where $\vec{F}_{p_{j|i}}$ is the pressure force of particle $j$ in respect to particle $i$ and $\vec{r}'_j$ is its new position.This change only is valid if the difference between $|F^C_{p_{j|i}}|$ and $|F^C_{p_{j|i}}|$ is lower than $5\%$. Although this limitation seems restrictive, as the pressure force control the incompressibility, it allows us that the difference between two forces is lower than this value.

## 5 Results

In this section, we will carry out a set of tests to show the improvements that offer our proposal. To that end, we will simulate a fluid whose dynamic is described by the equations (7) and (8). To solve this system of equations, it will be regarded the techniques MPM [21], GSPH [7] and P–SPH. The aim is to compare the obtained results from each technique to show the improvement that can be obtained by the proposed technique. It will be implemented three tests commonly used to quantify the stability and accuracy [24, 26, 27], these are: *settling of a random particles distribution*, *Sod's shock–tube* and *blast–wave*. In each test, we will carry out an analysis of the range of the number of neighbour particles where each technique is stable.

We have regarded the most of the values of simulation parameters suggested by [24]. Each test has different values that be specified in each simulation. Nevertheless, in all them, the value of the adiabatic parameter $\gamma$, equation (9), will be $\gamma = 1,46$. Regarding our proposed pressure force, equation (13), the selected values of $\varepsilon$ and $\zeta$ are $\varepsilon = 0.45$ and $\zeta = 1.0$. Likewise, all simulations will be implemented using a Wendland $C^4$ as kernel function. We have selected this function due to its analytic features that favour the stability and accuracy, according is highlighted by [3].

### 5.1 Settling of a Random Particles Distribution

Several research show a consensous which regards the settling of a random particle distribution as a suitable test to quantify the stability in SPH [3, 21, 29]. Descriptively, in this test, a particles system evolve from

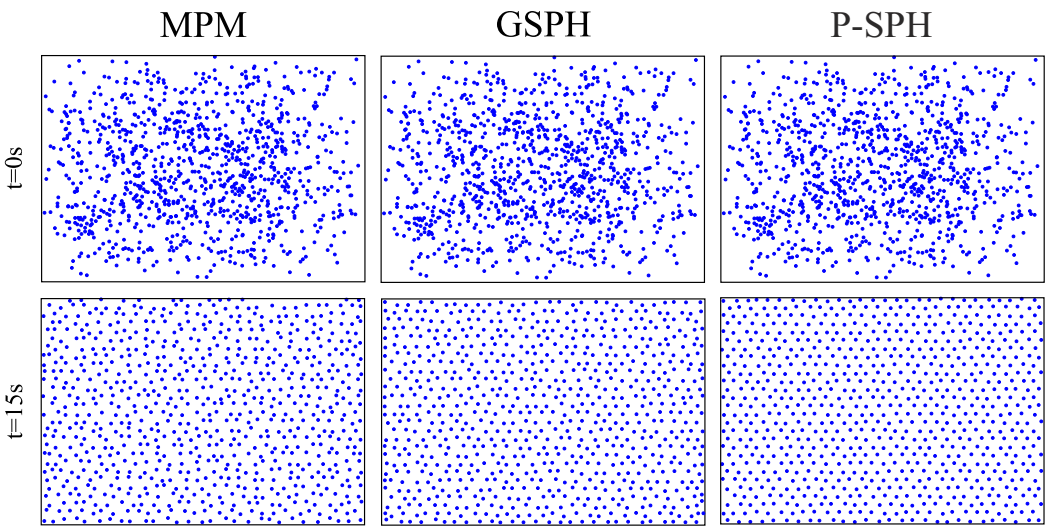


Figure 2: Evolution from a random particles distribution to a settled particles distribution.

a random distribution to a state that shows a level of regularity. The achieved regularity allows quantifying the stability degree of any SPH simulation [21, 24].

To implement this test, we have used 980 particles whose mass is $m = 0.00213$. The simulation limits are $[50 \times 30]$ and the time step used $\Delta t = 1.5\,10^{-4} s$ and $h = 0.023$. From this values, we have obtained the simulation shown in Figure 2.

To analyse the range of the number of neighbour particle that allow obtaining stable and accuracy simulation, we have changed from the lowest number to highest. In this test, the used values are:

| | MPM | GSPH | P–SPH |
|---|---|---|---|
| $N_i$ | 120–375 | 95–375 | 15–375 |
| $\mathcal{N}_i$ | 180 | 165 | 25 |

Table 1: Range of the number of neighbour particles. $N_i$ refers to range that allows stability and $\mathcal{N}_i$ is the value regarded to obtain the simulations shown in Figure 2.

From the Figure 2, we can say that the best result is obtained from P–SPH. This one allows obtaining the results of the highest regularity. To quantify this lattice degree, we have formulated an *order parameter* $\varsigma$ that satisfies:

$$\varsigma = \frac{\sum_{k=1}^{s}(|d^l - d_{ij}^k|)}{s}, \qquad (17)$$

where $s = (m-1)(n-1)$, and $m$ and $n$ are the particles number in each space direction, $d^l$ is the lattice length, $d_{ij}^k$ is the distance between each pair of neighbour particles. From the formulation of the parameter $\varsigma$, it can be said that the lower value, the more lattice degree is achieved and, consequently, the more stability is obtained.

The obtained values of this parameter are shown in Table 2.

| | MPM | GSPH | P–SPH |
|---|---|---|---|
| $\varsigma$ | 21.7 | 16.4 | 4.7 |

Table 2: Obtained values of the order parameter from Figure 2.

## 5.2 Sod's Tube–Shock Test

Sod's shock–tube test [27] allow quantifying the accuracy and stability of SPH [10, 14, 26]. Descriptively, the shock–tube test is built by a tube where a non–porous membrane is introduced. This membrane defines two sections that are filled with gas. In a section, that is named as *high section*, the gas is around 10 times denser and more confined than in the other section which is named *low section*. From these initial constraints, the membrane is instantly taken away, at $t = 0$. At this moment, due to differences of pressure and density between high–low sections, a shock wave is generated. This one evolves into the low section. At the same time, a rarefaction wave appears into the high section. Between each wave, a contact discontinuity is arisen. Quantitetively, from the obtained accuracy in the simulation of these three regions, it is possible to quantify the suitability of the used technique.

To carry out this test we have used a domain $[\text{-}0.5, 0.5]$. The low section is limited between $[\text{-}0.5, 0.0)$ and the high section is limited by

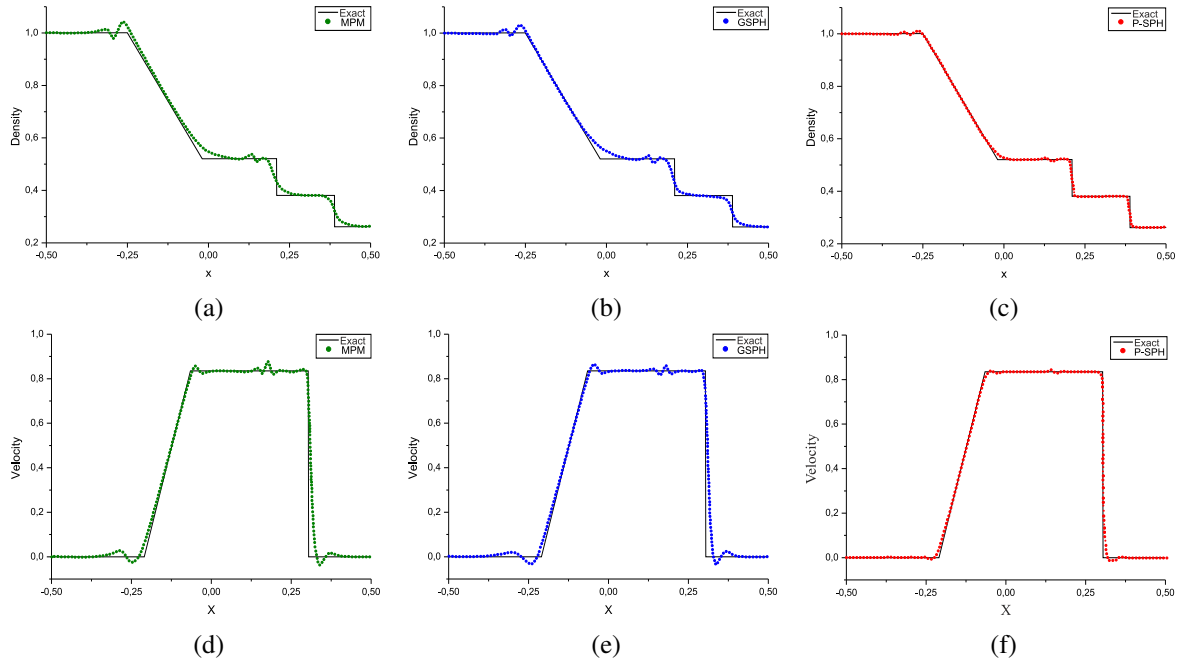


Figure 3: Comparative graphs of the exact solution and numerical obtained values from MPM, GSPH and P-SPH for Sod's shock–tube test.

$(0.0, 0.5]$. The remaining used paremeters are the suggested by [24].

From these initial values, we have obtained the results shown in Figure 3 at time $t = 0.15$. It is regarded the density and the velocity to evaluate the obtain accuracy, according to the suggestion given by [24, 26].

The Figure 3 shows a comparison between the exact solution, solid line, and the numerical solution shows as dots.

In each graphs, it is possible to identify three region: *the contact discontinuity*, *the rarefaction wave* and *the shock wave*. The contact discontinuity appears around $x_{cd} = 1.004$, the rarefaction wave appear from $x < x_{cd}$ and the shock wave from $x > x_{cd}$. Although the position of the contact discontinuity is the same in all graphs, both the spatial width of the contact discontinuity and its waving, shows significant discrepancies.

To quantify the obtained accuracy, we have selected the numeric values of each part of the flow, i.e., rarefaction wave, contact discontinuity and shock wave, specifically the width that are appointed as: $W_{rt}$ the width of the rarefaction tail, $W_{cd}$ the width of contact discontinuity and $W_{sw}$ the width of the shock wave. The obtained values are shown in Tables 3 and 4.

| | MPM | GSPH | P–SPH |
|---|---|---|---|
| $r^2$ | 0.9651 | 0.9708 | 0.9891 |
| $W_{rt}$ | 0.105 | 0.073 | 0.0205 |
| $W_{cd}$ | 0.078 | 0.061 | 0.026 |
| $W_{sw}$ | 0.128 | 0.104 | 0.051 |

Table 3: The most relevant values associated with the density graphs of Sod's shock–tube test, Figs. 3a, 3b and 3c.

| | MPM | GSPH | P–SPH |
|---|---|---|---|
| $r^2$ | 0.9651 | 0.9688 | 0.9891 |
| $W_{rt}$ | 0.126 | 0.099 | 0.039 |
| $W_{cd}$ | 0.101 | 0.075 | 0.043 |
| $W_{sw}$ | 0.089 | 0.065 | 0.037 |

Table 4: The most relevant values associated with the velocity graphs of Sod's shock–tube test, Figs. 3d, 3e and 3f.

## 5.3 Blast–Wave Test

The blast–wave test is a more extreme version of Sod's shock–tube test and is formulated for a very high Mach number, around $M = 200$. It was developed by Woodward and Colella [31] to highlight the behaviour of the contact discontinuity, mainly for the velocity, at high density and pressure values. In blast–wave test, the flow evolution shows the same features that Sod's shock–tube test, namely, a contact discontinuity will appear inserted between the shock wave and the rarefaction wave.

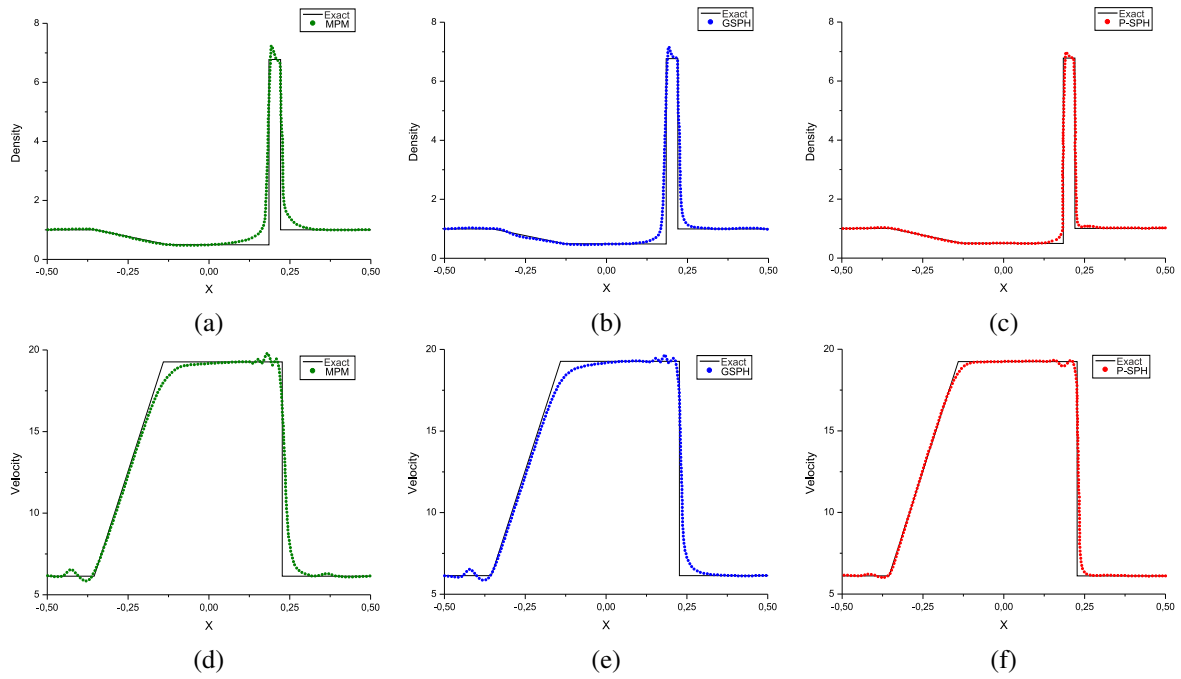


Figure 4: Comparative graphs of the exact solution and numerical obtained values from MPM, GSPH and P-SPH for blast–wave test.

As a result of the similarities with Sod's shock–tube test, we have only changed the initial values of some simulation parameters. The new values of mass density, pressure and thermal energy are: $(\rho_h, p_h, u_h) = (1.0, 1\,10^3, 0.0)$ and $(\rho_l, p_l, u_l) = (1.0, 0.01, 0.0)$, according to the suggestions given by [26, 31]. The new time step is $\Delta t = 8\,10^{-5}$. Using these values, we have obtained the results that are shown in Figure 4 at time $t = 7.5\,10^{-4}$, where the exact solutions and numeric solutions are depicted by solid line and dots, respectively.

Similarly to Sod's shock–tube test, the three regions that arise when the membrane is taken away can be located in the graphs of Figure 4: the contact discontinuity position $x_{cd} = 0.1081$, the rarefaction wave $x < x_{cd}$ and the shock wave $x > x_{cd}$. Likewise, in each graph of 4 the width of contact discontinuity changes for technique obtaining the lowest width when our proposal is implemented.

Analogously as the previous section 5.2 to shown the obtained accuracy, we have selected the most relevant values associated to the graphs of 4. These values are shown in Tables 5 and 6.

| | MPM | GSPH | P–SPH |
|---|---|---|---|
| $r^2$ | 0.9618 | 0.9791 | 0.9903 |
| $W_{rt}$ | 0.094 | 0.081 | 0.046 |
| $W_{cd}$ | 0.035 | 0.018 | 0.009 |
| $W_{sw}$ | 0.094 | 0.079 | 0.038 |

Table 5: The most relevant values associated with the density graphs of blast–wave shock test, Figs. 4a, 4b and 4c.

| | MPM | GSPH | P–SPH |
|---|---|---|---|
| $r^2$ | 0.9621 | 0.9788 | 0.9901 |
| $W_{rt}$ | 0.0945 | 0.0813 | 0.0585 |
| $W_{cd}$ | 0.0826 | 0.0582 | 0.0348 |
| $W_{sw}$ | 0.087 | 0.026 | 0.009 |

Table 6: The most relevant values associated with the velocity graphs of blast–wave test, Figs. 4d, 4e and 4f.

## 6 Conclusions

In this paper, we have reviewed some of the most relevant features that influence on the accuracy and stability of flow simulation by SPH. From these features, we have proposed a hybrid potential–SPH based method. To show the improvements obtained by the proposed technique, we have implemented a set of tests using an incompressible and inviscid fluid. In each implemented test we have compared our proposal with the MPM and GSPH techniques which are formulated to avoid the instabilities related to the pressure gradient. Particularly, analysing the tests' results,

we can conclude:

1. The P-SPH technique allows us to obtain a high stability. This conclusion can be deduced from the obtained results in settling test, Figure 2, where the obtained results by P-SPH show greater lattice degree than the obtained ones by the other two techniques. Quantitatively, this improvement is shown by the results of the parameter $\varsigma$, Table 2, where the obtained values by P-SPH are the lowest ones.

2. The P-SPH allow us to obtain highly accurate results in simulations where the shock wave and contact discontinuity appear. This affirmation is based on the obtained results in Sod's shock–tube test. The obtained graphs of the density and velocity, Figure 3, are more accurately simulated by P-SPH than by MPM or GSPH. This accuracy is more apparent in the rarefaction tail, the contact discontinuity and the shock wave. To reinforce this fact, we have selected the values associated to these regions that are shown in Tables 3 and 4. All obtained values evidence that the best accuracy is offered by P-SPH.

3. The improvements obtained in Sod's shock–tube test is also accomplished in a more extreme version of this test. This conclusion can be obtained from the results shown in the blast–wave test. Qualitatively, the obtained results are in agreement with the exact solutions. Nevertheless, the most accurate results are obtained by the P-SPH, as can be seen in the graphs of Figure 4. Quantitatively, the improvement is shown in the values of Tables 5 and 6.

4. The P-SPH allow us to obtain stable simulations for a wide range of the number of neighbour particles. Also, the stability is achieved with the lowest number, as consequence. The P–SPH not only favour the stability but also the efficiency, from the computational cost point of view. This conclusion can be deduced from Table 1.

From these results, we can conclude that the P-SPH improves both the stability and the accuracy of fluid flow simulations by SPH

**Acknowledgements:** This research has been supported by the Pololas project (TIN2016-76953-C3-2-R) of the Spanish Ministry of Economy and Competitiveness.

*References:*

[1] R. M. Cabezón, D. García-Senz, and A. Relano. A one–parameter family of interpolating kernels for smoothed particle hydrodynamics studies. *Journal of Computational Physics*, 227(19):8523–8540, Oct 2000.

[2] S. J. Cummins and R. M. An improved sph method for modeling liquid sloshing dynamics. *Journal of Computational Physics*, 152:584–607, Jul 1999.

[3] W. Dehnen and H. Aly. Improving convergence in smoothed particle hydrodynamics simulations without pairing instability. *Monthly Notices of the Royal Astronomical Society*, 425(2):1068–1082, Apr 2012.

[4] C. T. Dyka, P. W. Randles, and R. P. Ingel. Stress points for tension instability in sph. *International Journal for Numerical Methods in Engineering*, 40(13):2325–2341, Jul 1997.

[5] R. Gingold and J. Monaghan. Smoothed particle hidrodynamics: Theory and application to non–spherical stars. *Royal Astronomical Society*, 181:375–389, 1977.

[6] M. Ihmsen, J. Orthmann, B. Solenthaler, A. Kolb, and M. Teschner. Sph fluids in computer graphics. In *Eurographics 2014 - State of the Art Reports*. The Eurographics Association, 2014.

[7] S. Inutsuka. Reformulation of smoothed particle hydrodynamics with riemann solve. *Journal of Computational Physics*, 179(1):238–267, Jun 2012.

[8] K. Iwasaki and S. Inutsuka. Smoothed particle magnetohydrodynamics with a riemann solver and the method of characteristics. *Monthly Notices of the Royal Astronomical Society*, 418(3):1668–1688, Dec 2011.

[9] G. Liu and M. Liu. *Smoothed Particle Hydrodynamics:A Meshfree Particle Method*. World Scientific, 2003.

[10] M. Liu, G. Liu, and K. Lam. Constructing smoothing functions in smoothed particle hydrodynamics with applications. *Journal of Computational and Applied Mathematics*, 155(2):263–284, Jun 2003.

[11] L. B. Lucy. A numerical approach to the testing of the fission hypothesis. *Astronomical Journal*, 82(12):1013–1024, Dec 1977.

[12] M. Macklin and M. Müller. Position based fluids. *ACM Transactions on Graphics*, 32(4):104:1–104:12, Jul 2013.

[13] J. Monaghan. Smoothed particle hydrodynamics. *Annual Review of Astronomy and Astrophysics*, 30:543–574, Dec 1992.

[14] J. Monaghan. Sph without a tensile instability. *Journal of Computational Physics*, 159(2):290–311, May 2000.

[15] J. Monaghan. Smoothed particle hydrodynamics. *Rep. Prog. Phys.*, 68(8):1703–1759, Jul 2005.

[16] J. Monaghan. A turbulence model for smoothed particle hydrodynamics. *European Journal of Mechanics–B Fluids*, 30(4):360–370, Jul-Aug 2011.

[17] J. Morris. A study of the stability properties of smooth particle hydrodynamics. *Publications Astronomical Society of Australia*, 13(1):97–102, Feb 1995.

[18] J. Morris. Analysis of smoothed particle hydrodynamics with applications. *Monash University*, 13, Jul 1996.

[19] M. Müller, D. Charypar, and M. Gross. Particle-based fluid simulation for interactive applications. In *Proceedings of the 2003 ACM SIGGRAPH/Eurographics symposium on Computer animation*, SCA '03, pages 154–159, 2003.

[20] C. Nguyen, C. Nguyen, H. Bui, C. Nguyen, and R. Fukagawa. A new sph-based approach to simulation of granular flows using viscous damping and stress regularisation. *Landslides*, 14(1):69–81, Feb 2017.

[21] D. J. Price. Smoothed particle hydrodynamics and magnetohydrodynamics. *Journal of Computational Physics*, 231(3):759–794, Dec 2012.

[22] D. J. Price and J. J. Monaghan. Smoothed particle magnetohydrodynamics-i. algorithm and tests in one dimension. *Monthly Notices of the Royal Astronomical Society*, 348(1):123–138, Feb 2004.

[23] K. Puri and P. Ramachandran. Approximate riemann solvers for the godunov sph (gsph). *Journal of Computational Physics*, 270(Supplement C):432–458, Aug 2014.

[24] K. Puri and P. Ramachandran. A comparison of sph schemes for the compressible euler equations. *Journal of Computational Physics*, 256(0):308–333, Jan 2014.

[25] J. I. Read, T. Hayfield, and O. Agertz. Resolving mixing in smoothed particle hydrodynamics. *Monthly Notices of the Royal Astronomical Society*, 405(3):1513–1530, Jun 2010.

[26] L. Sigalotti and H. López. Adaptive kernel estimation and sph tensile instability. *Computers & Mathematics with Applications*, 55(1):23–50, Jan 2008.

[27] A. Sod. A survey of several finite difference methods for systems of nonlinear hyperbolic conservation laws. *Journal of Computational Physics*, 27(1):1–31, Jun 1978.

[28] B. Solenthaler and R. Pajarola. Predictive-corrective incompressible sph. *ACM Transactions Graphics*, 28(3):41–46, Jul 2009.

[29] V. Springel. Smoothed particle hydrodynamics in astrophysics. *Annual Review of Astronomy and Astrophysics*, 48(1):391–430, Sep 2010.

[30] K. Sugiura and S. Inutsuka. An extension of godunov sph ii: Application to elastic dynamics. *Journal of Computational Physics*, 333(Supplement C):78–103, Mar 2017.

[31] P. Woodward and P. Colella. The numerical simulation of two–dimensional fluid flow with strong shocks. *Journal of Computational Physics*, 54(1):115–173, 1984.

[32] X. Yang, S. Peng, and M. Liu. A new kernel function for sph with applications to free surface flows. *Applied Mathematical Modelling*, 38(15-16):3822–3833, Aug 2014.

[33] Y. Yasmin Melen, L. G. Sigalotti, and A. Hasmy. On the {SPH} tensile instability in forming viscous liquid drops. *Computer Physics Communications*, 157(3):191–200, Mar 2004.

[34] O. C. Zienkiewicz, R. L. Taylor, and P. Nithiarasu. *The Finite Element Method for Fluid Dynamics*. Elsevier B.V, $7^{th}$ ed. edition, 2014.